HHS Public Access

Author manuscript

J Phys Chem Lett. Author manuscript; available in PMC 2019 August 21.

Published in final edited form as:

J Phys Chem Lett. 2018 August 02; 9(15): 4239–4244. doi:10.1021/acs.jpclett.8b01723.

Contact Line Pinning Is Not Required for Nanobubble Stability on Copolymer Brushes

David S. Bull, **Nathaniel Nelson**, **Danielle Konetski**, **Christopher N. Bowman**, **Daniel K. Schwartz**, **Andrew P. Goodwin***

Department of Chemical and Biological Engineering, University of Colorado, Boulder, Colorado 80309, United States

Abstract

Whereas nanobubble stability on solid surfaces is thought to be based on local surface structure, in this work, we show that nanobubble stability on polymer brushes does not appear to require contact-line pinning. Glass surfaces were functionalized with copolymer brushes containing mixtures of hydrophobic and hydrophilic segments, exhibiting water contact angles ranging from 10 to 75°. On unmodified glass, dissolution and redeposition of nanobubbles resulted in reformation in mostly the same locations, consistent with the contact line pinning hypothesis. However, on polymer brushes, the nucleation sites were random, and nanobubbles formed in new locations upon redeposition. Moreover, the presence of stable nanobubbles was correlated with global surface wettability, as opposed to local structure, when the surface exceeded a critical water contact angle of 50 or 60° for polymers containing carboxyl or sulfobetaine groups, respectively, as hydrophilic side chains. The critical contact angles were insensitive to the identity of the hydrophobic segments.

Graphical Abstract

*Corresponding Author andrew.goodwin@colorado.edu.

ASSOCIATED CONTENT

Supporting Information

The Supporting Information is available free of charge on the ACS Publications website at DOI: 10.1021/acs.jp-clett.8b01723.

Detailed description of materials and methods, TIRF microscopy schematic, additional TIRF micrographs, and surface characterization data (PDF)

The authors declare no competing financial interest.

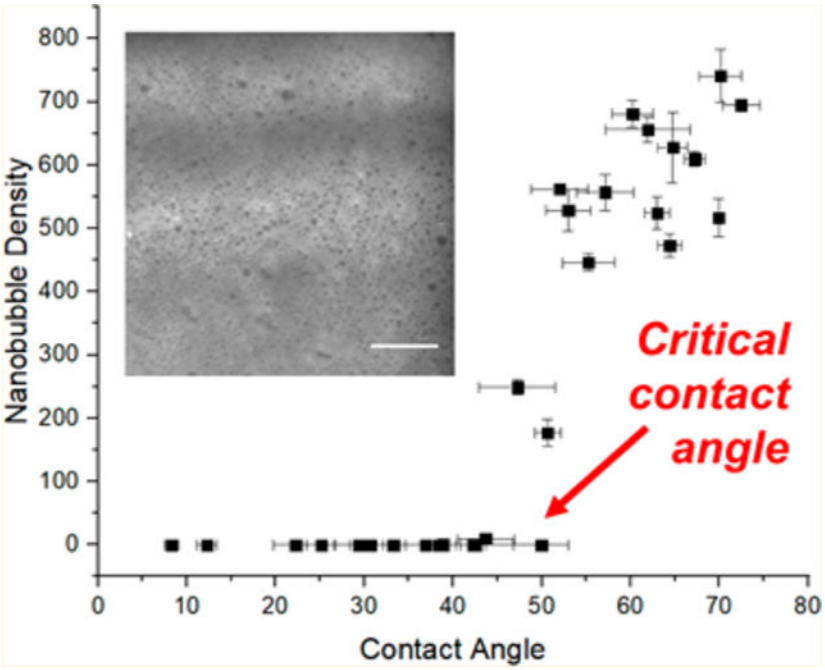

Surface nanobubbles are small, stable gas pockets that may be present at a solid–liquid interface, with dimensions on the order of tens of nanometers in height and hundreds of nanometers in diameter.[2,3] The presence of gas has been confirmed by a variety of characterization methods, including atomic force microscopy,[1,4] attenuated total reflectance infrared spectroscopy,[5] total internal reflection microscopy (TIRF),[6] and others.[7–12] Nucleation of surface nanobubbles generally occurs through supersaturation of gas at a liquid–solid interface, through either direct immersion of a surface in water[4] or solvent exchange from a solvent with higher gas solubility.[13] This process is followed by growth from dissolved gas controlled by either gas saturation or temperature.[14–16] For a small radius of curvature, the high Laplace pressure would predict that very high supersaturation ratios would be required for stability, yet despite Laplace pressures estimated at tens of megapascals, surface nanobubbles have been recorded to be stable for days at a time,[2] thus appearing to defy conventional interfacial thermodynamics.[3,17,18]

One of the key hypotheses for nanobubbles' exceptional stability is pinning of nanobubble contact line due to surface topography or the presence of contaminants.[18] Pinning, or fixation of the contact line by a topological defect, is a commonly found when liquid is added to an air–solid interface through either liquid transfer or nucleation.[19–21] Under supersaturated conditions,[22] one might expect a coarsening process, as observed for bubbles dispersed in a bulk liquid, where large (less-curved) bubbles grow at the expense of small (more-curved) bubbles and there is no stable bubble size. However, if a bubble's contact line is pinned, then bubble growth increases curvature. Experimentally, it has been rigorously shown that nanobubbles can be stable under these conditions.[22,23]

On solid surfaces, there is considerable experimental evidence to support the pinning hypothesis.[16,24] For example, whereas surface-bound nanobubbles would be expected to be

spherical caps, irregular shapes have also been imaged that could be explained by topography in the underlying surface structure.[1] Pinning would also help to explain apparent discrepancies in observations of nanobubble stability on various solid surfaces. In general, nanobubbles have been found to be stable on hydrophobic and unstable on hydrophilic surfaces;[10] however, various groups have reported the presence of stable nanobubbles on gold surfaces with receding contact angles ranging from 107 (hydrophobic) to 15° (hydrophilic).[25,26] Many studies have shown that whereas alkylated silica serves as a convenient surface for nanobubble study, nanobubbles have also been detected on bare glass.[6] The effect of surface roughness is also debatable: Although defect sites appear to promote stability, nanobubbles have also been found on hydrophilic, flat mica.[27] In addition, nanobubbles have been observed on highly ordered pyrolytic graphite (HOPG) but not amorphous glassy carbon.[28] Interestingly, McKinley and coworkers showed that nanobubbles could be confined to hydrophobic domains on a photopatterned polymer surface,[29] but to our knowledge no systematic study has been performed describing the effect of copolymer structure on nanobubble stability.

In this work, we present evidence that nanobubbles can indeed be stabilized on homogeneous dynamic copolymer brush surfaces, even in the absence of strong pinning sites. Because macromolecules can continuously reconfigure their conformations to balance osmotic pressure and chain entropy, structural defects necessary for pinning are transient, if present at all. Thus, whereas nanobubbles repeatedly form in the same locations on silane-functionalized glass (presumably at defect sites that promote strong pinning), here we show that on polymer surfaces they form in random locations with no correlation to previous nucleation events. The hydrophobicity of the brushes was systematically adjusted by synthesizing copolymers with a controlled ratio of hydrophilic to hydrophobic side chains. Interestingly, we found that a critical hydrophobicity (as determined by water contact angle) was required for nanobubble stability on these polymer surfaces, the value of which depended on the underlying polymer structure. Above this contact angle, hundreds of nanobubbles were imaged over a 1000 μm^2 area, but below this angle no nanobubbles were found. Even partially wetting surfaces, in some cases with receding contact angles <50°, were found to stabilize nanobubbles. Thus, in contrast with typical solid surfaces that possess defect sites that are unpredictable and difficult to control, the conditions under which nanobubbles are stable on copolymer brushes are repeatable and tunable. The ability to understand and control surface nanobubble stability will have an impact on the design of materials for a wide range of important applications, including froth flotation,[30–33] surface cleaning,[34,35] hydrodynamic boundary slip,[36] photoacoustic imaging,[37] enhanced adhesion, and nonfouling surfaces.[38,39]

To obtain fine control and consistency over surface properties, polymers were grown directly from surfaces using atom transfer radical polymerization (ATRP). ATRP utilizes a copper-bromide equilibrium to eliminate termination steps, thereby assuring a copolymer brush with consistent composition. Polymers grown on a surface by ATRP have been shown to be consistent in composition and molecular weight dispersity with those found in the same polymers synthesized in bulk, so accurate predictions can be made about the resultant surface properties.[40] To allow polymerization from the surface, cleaned glass slides were functionalized with 3-aminopropyltriethoxysilane (APTES) and α-bromoisobutyryl bromide

(BIBB) in successive steps, resulting in the formation of surfaces with $\theta \approx 60$ and 75°, respectively. Successful conjugation was also confirmed by ellipsometry measurements of analogous reactions on a silicon wafer, which showed successive increases in surface thickness of 2.0 to 3.5 and 1.3 nm for APTES and BIBB, respectively. Each advancing contact-angle measurement was run in at least three locations on each surface, where error was ~5° for most surfaces.

Once the surfaces were prepared, nanobubbles were formed by a solvent-exchange method on functionalized glass surfaces and imaged in situ by TIRF microscopy, which allowed imaging directly in the flow chamber during solvent exchange (Figure S1). To confirm the presence of nanobubbles, glass coverslips (40 × 22 × 0.1 mm) were first methylated with hexamethyldisilazane (HMDS) to create a hydrophobic surface that has been reported to support nanobubble stability.[10,41] The coverslip was then placed in a flow chamber and mounted on the TIRF microscope stage (Figure S1). An air-saturated ethanolic solution of AlexaFluor 488 (AF488) was flowed onto a glass surface, followed by exchange with air-saturated water. The rapid decrease in air solubility from ethanol to water caused nucleation of gas pockets on the surface. These gas pockets prevented AF488 intrusion, which created voids in the TIRF microscope image (Figure 1 and Figure S2). AF488 was an ideal choice because of its net negative charge, low surface activity, and stability against photobleaching. Several previous reports utilized Rhodamine 6G as a fluorescent contrast marker;[6,42–44] however, in our experiments, the positively charged Rhodamine 6G appeared to adhere to the negatively charged glass surfaces, and it was difficult to determine whether the nanobubbles were forming on the functionalized glass or on adsorbed rhodamine islands (Figure S3). Images were analyzed using an edge detection MATLAB code. Because of concerns about achieving accurate nanobubble size measurements near the diffraction limit, nanobubble count per area was used as a metric for evaluating nanobubble stabilization rather than area fraction or nanobubble size.

The differences between nanobubbles formed on organosilane-functionalized glass as compared with polymer brushes were elucidated by a series of repeated nanobubble deposition and dissolution experiments. After nanobubbles were deposited by solvent exchange from air-saturated ethanol to water, the process was reversed by exchanging with ethanol again, followed by an exchange with degassed water, which was expected to result in bubble dissolution. No nanobubbles were found after surface immersion in degassed water, which was consistent with previous reports.[10] This observation confirms that the features observed in microscope images were indeed composed of gas rather than a contaminant or silicone oil from the syringe and tubing assembly.[10,45] When the methylated glass surfaces were subsequently exposed to air-saturated ethanol and air-saturated water, the nanobubbles reformed in the same or similar locations as prior to degassing, as shown in representative images (Figure S4). Using an algorithm to colocalize the two images, the Pearson correlation coefficient (PCC) for the nanobubbles reforming on a methylated glass surface was found to be 0.69 (Figure 2), indicating a strong inclination to form bubbles in the same locations. This observation was consistent with studies by Lohse and coworkers, who showed that nanobubbles appeared in the same locations on methylated glass surface even after cavitation with high-intensity focused ultrasound.[46] Importantly, the same solvent-exchange process performed for surfaces with methacrylic acid-*co*-methyl methacrylate

(MAA-*co*-MMA) polymer brushes led to the formation of nanobubbles in apparently random locations (Figure 2, PCC = 0.16). We hypothesize that defect sites on silane-modified silica surfaces were present that were conducive to nanobubble stabilization, and these isolated sites consistently stabilized bubbles in independent depositions. In contrast, polymer brushes fully covered the surface, as supported by film thicknesses from 7 to 80 nm (Table S1), and provided a much more homogeneous substrate, consistent with the molecular-level dynamic nature of polymer chains; any defects that might have stabilized nanobubbles were expected to be transient and to heal over time.

To determine the relationship between nanobubble stability and surface hydrophobicity, we synthesized brushes composed of random copolymers of methacrylic acid (MAA) and methyl methacrylate, adjusting the feed ratios from 0 to 100 to achieve a range of receding water contact angles (θ) from 30 to 70°, respectively (Figure S5). Dynamic contact-angle measurements showed a difference of about 25–35° between advancing and receding contact angles, which is consistent with literature reports for measurements on copolymer surfaces (Figure S6).[47,48] When surfaces with MAA-*co*-MMA were subjected to solvent exchange, nanobubble stability was only supported once a critical surface hydrophobicity was reached (Figure 3). For ten MAA-*co*-MMA surfaces with $\theta < 44°$, none had more than one nanobubble. In contrast, for the 13 surfaces analyzed for $\theta > 50°$, all but one had at least 450 nanobubbles per 1000 μm^2. The presence of the AF488 did not affect the measured contact angle (Figure S7). The four surfaces measured between 44 and 50° showed various nanobubble counts over a 1000 μm^2 area, including (44°, 10), (47°, 249), (50°, 0), and (51°, 177); from these results, we assign a critical contact angle of 48 ± 5°. Data obtained using different synthesis batches and on different days still exhibited the same critical surface hydrophobicity, and nanobubbles were detected at the same locations 3 h postdeposition (Figure S8).

To ascertain the effects of polymer chemistry on nanobubble stability, polymers with zwitterionic side chains were employed in place of negatively charged MAA monomers; sulfobetaine methacrylate (SBMA) was copolymerized with MMA to form SBMA-*co*-MMA copolymers in a range of contact angles from 5 to 90° (Figure S5). When nanobubbles were formed on these surfaces, a similar trend appeared as for the MAA-*co*-MMA surfaces. In particular, for $\theta < 55°$, nine surfaces showed zero or one nanobubble, and one surface had 30 per 1000 μm^2 (Figure 3). When $\theta > 60°$, six of seven surfaces showed >270 nanobubbles per 1000 μm^2, whereas the other had only 36 nanobubbles per 1000 μm^2. As for the previous copolymer study, this result was obtained over different synthesis batches and performed on different days, showing the reproducibility and self-consistency of this system. Taking contact-angle measurement error into account, these surfaces appear to show a critical contact angle of ~62 ± 5°, which was 10–15° higher than for the MAA-*co*-MMA.

To test the potential effects of surface charge, we synthesized copolymers containing positively charged 2-(dimethylamino)-ethyl methacrylate (DMAEMA) as a hydrophobic component. Although DMAEMA contains a basic amine group, which has been utilized by others for inclusion of positive charge at neutral pH,[49] we found that DMAEMA copolymerization with either MAA or SBMA increased surface hydrophobicity, likely due

to the increased alkyl fraction of DMAEMA relative to the hydrophilic monomers. The results with DMAEMA matched closely with those using other copolymers. SBMA-*co*-DMAEMA exhibited a critical contact angle of ~62 ± 5°, consistent with SBMA-*co*-MMA. For comparison, surfaces functionalized with MAA-*co*-DMAEMA showed a critical contact angle between 40 and 55°. Unfortunately, this value could not be narrowed further due to contact-angle measurement uncertainty near this value, but this contact angle was generally consistent with the results found on MAA-*co*-MMA brushes. The self-consistency between experiments suggests that the hydrophilic component in the copolymer played a significant role in determining nanobubble stability on copolymer surfaces. As to the effect of hydrophilic side chain structure, Zhang and coworkers have suggested that water adsorbs strongly to SBMA zwitterions; perhaps this adhesion may induce an additional enthalpic penalty to water removal during nanobubble formation, thus requiring additional surface hydrophobicity to stabilize nanobubbles.[50] Whereas we do not have additional evidence to support this hypothesis, this theory is consistent with the observation that SBMA surfaces (θ < 10°) are more hydrophilic than MAA surfaces ($\theta \approx 30°$) (Figure S5).

Finally, the effect of surface charge was investigated as a potential factor in nanobubble stabilization, which is a plausible hypothesis given that bare bubbles in solution possess a negative zeta potential due to water ordering at the surface.[51–55] Because we prepared brushes with a wide range of cationic, neutral, and anionic side changes, we were able to empirically differentiate the potential effects of hydrophobicity and charge. The polymer brush surfaces were synthesized on standard glass microscope slides to allow measurement of surface zeta potential. By varying monomer composition, we obtained a large range of zeta potentials, from −40 to +25 mV (Figure S9). Interestingly, there did not appear to be a common critical zeta potential, suggesting that the charge was not as important a factor as surface hydrophobicity (Figure 4).

In this work, copolymer brushes were synthesized on surfaces to show how changes in surface hydrophobicity and surface charge affect nanobubble stability. Copolymers consisting of hydrophobic and hydrophilic monomers were grown from surfaces using ATRP. Nanobubbles were formed on these surfaces using a solvent-exchange method. After removing nanobubbles by water degassing, the new nanobubbles were found to form in different spots than those found originally, indicating that nanobubble stability was not dependent on underlying surface structure. By tuning the ratio of hydrophobic to hydrophilic monomers in the copolymers, it was found that nanobubbles required a critical hydrophobicity, as determined by contact angle, to maintain stability, and that the critical value of contact angle depended primarily on the detailed chemistry of the hydrophilic side chain. Surface charge was not correlated to nanobubble stability. This study suggests that nanobubbles on dynamic polymer surfaces do not require pinning for stability, which indicates a mechanism separate from nanobubbles on solid surfaces. Currently, we hypothesize that the dynamic polymer chains are able to distort their equilibrium packing to allow the nanobubble to adopt very low curvatures while preserving an equilibrium contact angle; however, testing this hypothesis will require further study. Taken together, these results have important implications for surface adhesion, membrane fouling, and other applications.

Supplementary Material

Refer to Web version on PubMed Central for supplementary material.

ACKNOWLEDGMENTS

Research was primarily supported by NIH DP2EB020401. D.K.S. and N.N. acknowledge funding from the U.S. Department of Energy Basic Energy Sciences, Chemical Science, Geoscience, and Bioscience Division (award DE-SC0001854) for the development of chemical imaging methods. We thank Prof. Ted Randolph for helpful suggestions and for use of his Surpass 3 instrument. We also thank Prof. Jennifer Cha, Hao Wu, Garret Chado, David Faulón Marruecos, and Dr. Ben Fairbanks for helpful discussions and Sarah Bull and Rebecca O'Toole for help with capturing images during TIRF microscopy studies.

REFERENCES

(1). Tyrrell JWG; Attard P Images of Nanobubbles on Hydrophobic Surfaces and Their Interactions. Phys. Rev. Lett. 2001, 87 (17), 176104.

(2). Lohse D; Zhang X Surface Nanobubbles and Nanodroplets. Rev. Mod. Phys. 2015, 87 (3), 981–1035.

(3). Borkent BM; Dammer SM; Schönherr H; Vancso GJ; Lohse D Superstability of Surface Nanobubbles. Phys. Rev. Lett. 2007, 98 (20), 204502.

(4). Ishida N; Inoue T; Miyahara M; Higashitani K Nano Bubbles on a Hydrophobic Surface in Water Observed by Tapping-Mode Atomic Force Microscopy. Langmuir 2000, 16 (16), 6377–6380.

(5). Zhang XH; Khan A; Ducker WA A Nanoscale Gas State. Phys. Rev. Lett. 2007, 98 (13), 136101.

(6). Chan CU; Ohl C-D Surface Nanobubble Nucleation Visualized with TIRF Microscopy. 2012, arXiv:1204.2633. arXiv.org e-Print archive. https://arxiv.org/abs/1204.2633.

(7). Zhang XH Quartz Crystal Microbalance Study of the Interfacial Nanobubbles. Phys. Chem. Chem. Phys. 2008, 10 (45), 6842–6848. [PubMed: 19015789]

(8). Martinez J; Stroeve P Transient Behavior of the Hydrophobic Surface/Water Interface: From Nanobubbles to Organic Layer. J. Phys. Chem. B 2007, 111 (51), 14069–14072. [PubMed: 18047320]

(9). Steitz R; Gutberlet T; Hauss T; Klösgen B; Krastev R; Schemmel S; Simonsen AC; Findenegg GH Nanobubbles and Their Precursor Layer at the Interface of Water Against a Hydrophobic Substrate. Langmuir 2003, 19 (6), 2409–2418.

(10). Switkes M; Ruberti JW Rapid Cryofixation/Freeze Fracture for the Study of Nanobubbles at Solid–Liquid Interfaces. Appl. Phys. Lett. 2004, 84 (23), 4759–4761.

(11). Zhang L; Zhao B; Xue L; Guo Z; Dong Y; Fang H; Tai R; Hu J Imaging Interfacial Micro- and Nano-Bubbles by Scanning Transmission Soft X-Ray Microscopy. J. Synchrotron Radiat. 2013, 20 (3), 413–418. [PubMed: 23592619]

(12). Karpitschka S; Dietrich E; Seddon JRT; Zandvliet HJW; Lohse D; Riegler H Nonintrusive Optical Visualization of Surface Nanobubbles. Phys. Rev. Lett. 2012, 109 (6), 066102.

(13). Lou S-T; Ouyang Z-Q; Zhang Y; Li X-J; Hu J; Li M-Q; Yang F-J Nanobubbles on Solid Surface Imaged by Atomic Force Microscopy. J. Vac. Sci. Technol., B: Microelectron. Process. Phenom. 2000, 18 (5), 2573–2575.

(14). Lhuissier H; Lohse D; Zhang X Spatial Organization of Surface Nanobubbles and Its Implications in Their Formation Process. Soft Matter 2014, 10 (7), 942–946. [PubMed: 24983101]

(15). Ishida N; Kusaka Y; Ushijima H Hydrophobic Attraction between Silanated Silica Surfaces in the Absence of Bridging Bubbles. Langmuir 2012, 28 (39), 13952–13959. [PubMed: 22931235]

(16). Yang J; Duan J; Fornasiero D; Ralston J Very Small Bubble Formation at the Solid–Water Interface. J. Phys. Chem. B 2003, 107 (25), 6139–6147.

(17). Epstein PS; Plesset MS On the Stability of Gas Bubbles in Liquid-Gas Solutions. J. Chem. Phys. 1950, 18 (11), 1505–1509.

(18). Ljunggren S; Eriksson JC The Lifetime of a Colloid-Sized Gas Bubble in Water and the Cause of the Hydrophobic Attraction. Colloids Surf., A 1997, 129–130, 151–155.

(19). Akbari A; Hill RJ Liquid-Bridge Stability and Breakup on Surfaces with Contact-Angle Hysteresis. Soft Matter 2016, 12 (32), 6868–6882. [PubMed: 27443494]

(20). Kumar S Liquid Transfer in Printing Processes: Liquid Bridges with Moving Contact Lines. Annu. Rev. Fluid Mech. 2015, 47 (1), 67–94.

(21). Snoeijer JH; Andreotti B Moving Contact Lines: Scales, Regimes, and Dynamical Transitions. Annu. Rev. Fluid Mech. 2013, 45 (1), 269–292.

(22). Lohse D; Zhang X Pinning and Gas Oversaturation Imply Stable Single Surface Nanobubbles. Phys. Rev. E 2015, 91 (3), 031003.

(23). Liu Y; Zhang X Nanobubble Stability Induced by Contact Line Pinning. J. Chem. Phys. 2013, 138 (1), 014706.

(24). Yang S; Tsai P; Kooij ES; Prosperetti A; Zandvliet HJW; Lohse D Electrolytically Generated Nanobubbles on Highly Orientated Pyrolytic Graphite Surfaces. Langmuir 2009, 25 (3), 1466–1474. [PubMed: 19123858]

(25). Song B; Walczyk W; Schönherr H Contact Angles of Surface Nanobubbles on Mixed Self-Assembled Monolayers with Systematically Varied Macroscopic Wettability by Atomic Force Microscopy. Langmuir 2011, 27 (13), 8223–8232. [PubMed: 21663323]

(26). Holmberg M; Kühle A; Mørch KA; Boisen A Nanobubble Trouble on Gold Surfaces. Langmuir 2003, 19 (25), 10510–10513.

(27). Zhang XH; Zhang XD; Lou ST; Zhang ZX; Sun JL; Hu J Degassing and Temperature Effects on the Formation of Nanobubbles at the Mica/Water Interface. Langmuir 2004, 20 (9), 3813–3815. [PubMed: 15875421]

(28). Zhang X; Maeda N Interfacial Gaseous States on Crystalline Surfaces. J. Phys. Chem. C 2011, 115 (3), 736–743.

(29). Agrawal A; Park J; Ryu DY; Hammond PT; Russell TP; McKinley GH Controlling the Location and Spatial Extent of Nanobubbles Using Hydrophobically Nanopatterned Surfaces. Nano Lett. 2005, 5 (9), 1751–1756. [PubMed: 16159218]

(30). Schubert H Nanobubbles, Hydrophobic Effect, Heterocoagulation and Hydrodynamics in Flotation. Int. J. Miner. Process. 2005, 78 (1), 11–21.

(31). Mishchuk N; Ralston J; Fornasiero D Influence of Very Small Bubbles on Particle/Bubble Heterocoagulation. J. Colloid Interface Sci. 2006, 301 (1), 168–175. [PubMed: 16725149]

(32). Ishida N Direct Measurement of Hydrophobic Particle-Bubble Interactions in Aqueous Solutions by Atomic Force Microscopy: Effect of Particle Hydrophobicity. Colloids Surf., A 2007, 300 (3), 293–299.

(33). Fan M; Tao D; Honaker R; Luo Z Nanobubble Generation and Its Applications in Froth Flotation (Part IV): Mechanical Cells and Specially Designed Column Flotation of Coal. Min. Sci. Technol. 2010, 20 (5), 641–671.

(34). Yang S; Duisterwinkel A Removal of Nanoparticles from Plain and Patterned Surfaces Using Nanobubbles. Langmuir 2011, 27 (18), 11430–11435. [PubMed: 21806003]

(35). Wu Z; Chen H; Dong Y; Mao H; Sun J; Chen S; Craig VSJ; Hu J Cleaning Using Nanobubbles: Defouling by Electrochemical Generation of Bubbles. J. Colloid Interface Sci. 2018, 328 (1), 10–14.

(36). Pan Y; Bhushan B; Zhao X The Study of Surface Wetting, Nanobubbles and Boundary Slip with an Applied Voltage: A Review. Beilstein J. Nanotechnol 2014, 5, 1042–1065. [PubMed: 25161839]

(37). Kim C; Qin R; Xu JS; Wang LV; Xu RX Multifunctional Microbubbles and Nanobubbles for Photoacoustic and Ultrasound Imaging. J. Biomed. Opt. 2010, 15 (1), 010510.

(38). Wu Z; Zhang X; Zhang X; Li G; Sun J; Zhang Y; Li M; Hu J Nanobubbles Influence on BSA Adsorption on Mica Surface. Surf. Interface Anal. 2006, 38 (6), 990–995.

(39). Carambassis A; Jonker LC; Attard P; Rutland MW Forces Measured between Hydrophobic Surfaces Due to a Submicroscopic Bridging Bubble. Phys. Rev. Lett. 1998, 80 (24), 5357–5360.

(40). Yadav V; Jaimes-Lizcano YA; Dewangan NK; Park N; Li T-H; Robertson ML; Conrad JC Tuning Bacterial Attachment and Detachment via the Thickness and Dispersity of a PH-Responsive Polymer Brush. ACS Appl. Mater. Interfaces 2017, 9 (51), 44900–44910. [PubMed: 29215264]

(41). Pan G; Yang B Effect of Surface Hydrophobicity on the Formation and Stability of Oxygen Nanobubbles. ChemPhysChem 2012, 13 (8), 2205–2212. [PubMed: 22271703]

(42). Chan CU; Chen L; Arora M; Ohl C-D Collapse of Surface Nanobubbles. Phys. Rev. Lett. 2015, 114 (11), 114505.

(43). Chan CU; Arora M; Ohl C-D Coalescence, Growth, and Stability of Surface-Attached Nanobubbles. Langmuir 2015, 31 (25), 7041–7046. [PubMed: 26039563]

(44). Hain N; Wesner D; Druzhinin SI; Schönherr H Surface Nanobubbles Studied by Time-Resolved Fluorescence Microscopy Methods Combined with AFM: The Impact of Surface Treatment on Nanobubble Nucleation. Langmuir 2016, 32 (43), 11155–11163. [PubMed: 27268423]

(45). Gerhardt A; Nguyen BH; Lewus R; Carpenter JF; Randolph TW Effect of the Siliconization Method on Particle Generation in a Monoclonal Antibody Formulation in Pre-Filled Syringes. J. Pharm. Sci. 2015, 104 (5), 1601–1609. [PubMed: 25740412]

(46). Bremond N; Arora M; Ohl C-D; Lohse D Cavitation on Surfaces. J. Phys.: Condens. Matter 2005, 17 (45), S3603.

(47). Hogt AH; Gregonis DE; Andrade JD; Kim SW; Dankert J; Feijen J Wettability and ζ Potentials of a Series of Methacrylate Polymers and Copolymers. J. Colloid Interface Sci. 1985, 106 (2), 289–298.

(48). Extrand CW; Kumagai Y An Experimental Study of Contact Angle Hysteresis. J. Colloid Interface Sci. 1997, 191 (2), 378–383. [PubMed: 9268520]

(49). Morrissey KL; He C; Wong MH; Zhao X; Chapman RZ; Bender SL; Prevatt WD; Stoykovich MP Charge-tunable Polymers as Reversible and Recyclable Flocculants for the Dewatering of Microalgae. Biotechnol Bioeng. 2015, 112 (1), 74–83. [PubMed: 25060233]

(50). He Y; Hower J; Chen S; Bernards MT; Chang Y; Jiang S Molecular Simulation Studies of Protein Interactions with Zwitterionic Phosphorylcholine Self-Assembled Monolayers in the Presence of Water. Langmuir 2008, 24 (18), 10358–10364. [PubMed: 18690732]

(51). Ushikubo FY; Enari M; Furukawa T; Nakagawa R; Makino Y; Kawagoe Y; Oshita S Zeta-Potential of Micro- and/or Nano-Bubbles in Water Produced by Some Kinds of Gases. IFAC Proc. Vol. 2010, 43 (26), 283–288.

(52). Cho S-H; Kim J-Y; Chun J-H; Kim J-D Ultrasonic Formation of Nanobubbles and Their Zeta-Potentials in Aqueous Electrolyte and Surfactant Solutions. Colloids Surf., A 2005, 269 (1), 28–34.

(53). Vàcha R; Rick SW; Jungwirth P; de Beer AGF; de Aguiar HB; Samson J-S; Roke S The Orientation and Charge of Water at the Hydrophobic Oil Droplet–Water Interface. J. Am. Chem. Soc. 2011, 133 (26), 10204–10210. [PubMed: 21568343]

(54). Tian CS; Shen YR Structure and Charging of Hydrophobic Material/Water Interfaces Studied by Phase-Sensitive Sum-Frequency Vibrational Spectroscopy. Proc. Natl. Acad. Sci. U. S. A. 2009, 106 (36), 15148–15153. [PubMed: 19706483]

(55). Gun'ko VM; Turov VV; Bogatyrev VM; Zarko VI; Leboda R; Goncharuk EV; Novza AA; Turov AV; Chuiko AA Unusual Properties of Water at Hydrophilic/Hydrophobic Interfaces. Adv. Colloid Interface Sci. 2005, 118 (1), 125–172. [PubMed: 16213452]

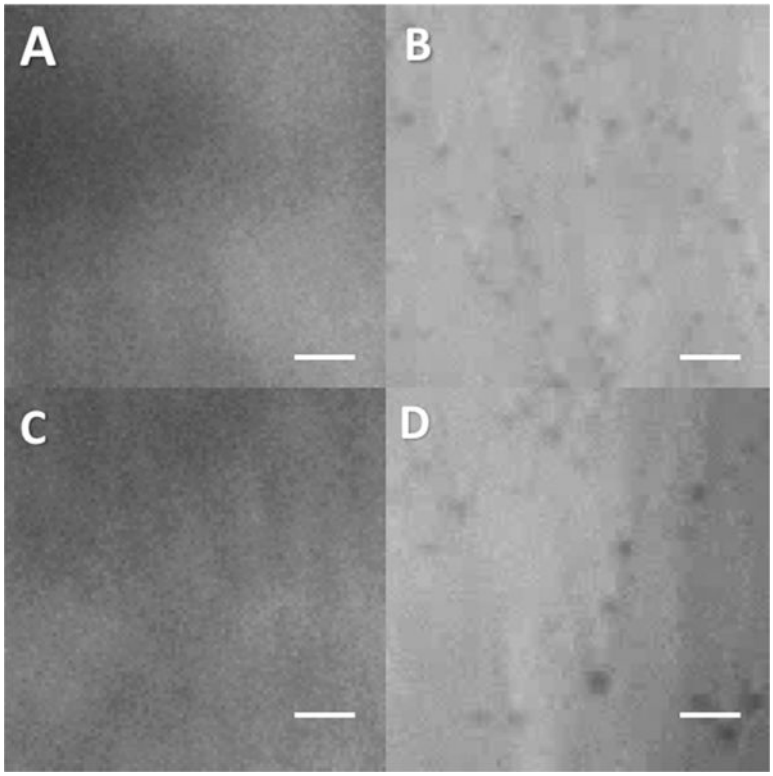

Figure 1.

TIRF images of nanobubble formation and dissolution on MAA-*co*-MMA surface. Images were acquired during the following sequence (note: all liquids contain AlexFluor488): rinse with ethanol (A), exchange to air-saturated water (B), exchange with ethanol and exchange to degassed water (C), exchange with ethanol and finally exchange with air-saturated water (D). Scale bar = 10 μm for all images.

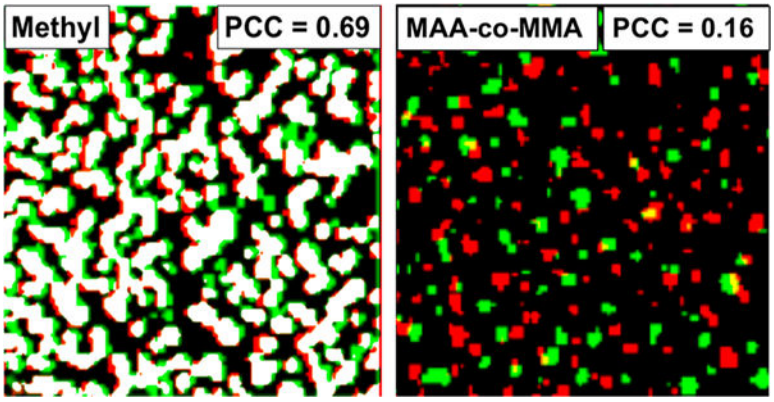

Figure 2.

Overlay of TIRF images for (left) methylated and (right) copolymer surfaces with nanobubbles formed (green), dissolved, and redeposited (red). Images have been Gaussian blurred and false colored; pixels with colocalization are white or yellow. The copolymer shown is MAA-*co*-MMA; PCC = Pearson correlation coefficient.

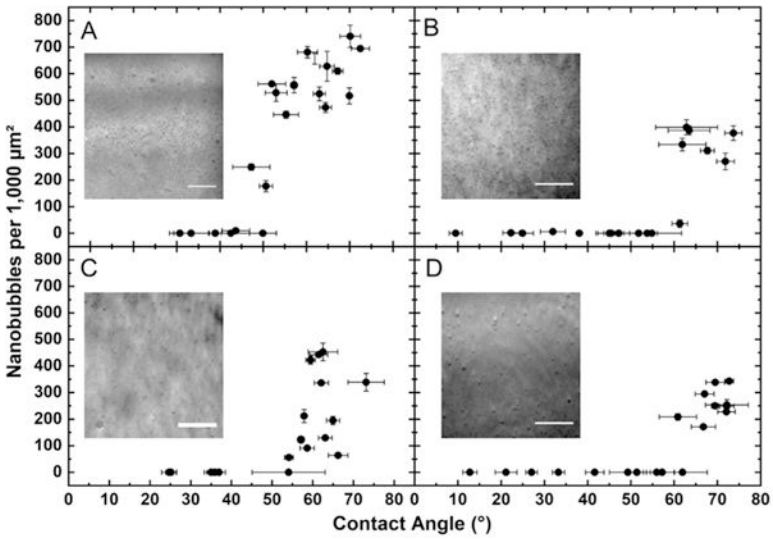

Figure 3.

Nanobubble density versus advancing contact angle for (A) MAA-*co*-MMA, (B) SBMA-*co*-MMA, (C) MAA-*co*-DMAEMA, and (D) SBMA-*co*-DMAEMA surfaces. Insets: representative TIRF images for each surface. Scale bar = 10 μm.

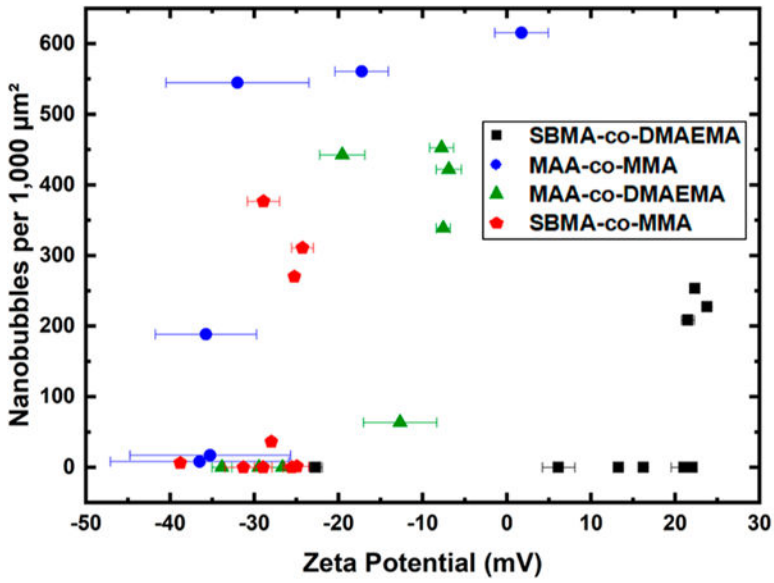

Figure 4.

Nanobubble density versus zeta potential of glass coverslips with copolymer coatings. The polymer coating formulations are the same as those shown in Figure 3.